BIOCHEMISTRY
including biophysical chemistry & molecular biology
Article

Biochemistry **2010,** *49,* 7839–7846 7839
DOI: 10.1021/bi100560q

Tyrosine 112 Is Essential for Organic Cation Transport by the Plasma Membrane Monoamine Transporter†

Horace T. B. Ho and Joanne Wang*

Department of Pharmaceutics, University of Washington, Seattle, Washington 98195

Received April 12, 2010; Revised Manuscript Received July 14, 2010

ABSTRACT: Plasma membrane monoamine transporter (PMAT) is a polyspecific organic cation transporter in the solute carrier 29 (SLC29) family. Previous studies suggested that the major substrate recognition sites are located within transmembrane domains (TM) 1−6, and interaction of PMAT with organic cations may involve aromatic residues. In this study, we analyzed the roles of tyrosine and tryptophan residues located within TM1−6 with a goal of identifying potential residues involved in substrate recognition and translocation. The six tyrosines and one tryptophan in this region were each mutated to alanine followed by analysis of the mutant's membrane localization and transport activity toward 1-methyl-4-phenylpyridinium (MPP^+), serotonin (5-HT), and dopamine. Two mutants, Y85A and Y112A, exhibited normal cell surface expressions but lost their transport activities toward organic cations. At position Y85, aromatic substitution with phenylalanine or tryptophan fully restored organic cation transport activity. Interestingly, at position Y112, phenylalanine substitution was not allowed. Tryptophan substitution at Y112 partially restored transport activity toward 5-HT and dopamine but severely impaired MPP^+ transport. Detailed kinetic analyses revealed that tryptophan substitution at Y85 and Y112 affected the apparent binding affinity (K_m) and maximal transport velocity (V_{max}) in a substrate-dependent manner. Together, our data suggest that Y85 and Y112 are important molecular determinants for PMAT function, and Y112 is indispensable for optimal interaction with organic cation substrates. Our analyses also suggest the involvement of transmembrane domains 1 and 2 in forming the substrate permeation pathway of PMAT.

The solute carrier 29 (SLC29) family consists of membrane transporters that mediate cellular uptake of important nutrients, signaling molecules, and therapeutic drugs (*1*, *2*). There are four *SLC29* gene isoforms, *SLC29A1*−*4*, in the human genome. *SLC29A1* and *SLC29A2* encode classic equilibrative nucleoside transporters 1 and 2 (ENT1[1] and ENT2, respectively), which transport purine and pyrimidine nucleosides and their structural analogues (*1*, *2*). ENT1 and ENT2 play important regulatory roles in nucleic acid synthesis and purinergic signaling pathways and are also important determinants of the cellular response to nucleoside drugs used in anticancer, antiviral, and immunosuppressive therapies (*1*, *2*). The third member, ENT3 (*SLC29A3*), also transports nucleosides and nucleoside analogues and mainly functions as an intracellular transporter (*3*, *4*). The fourth member, *SLC29A4*, was cloned and characterized in our laboratory as the plasma membrane monoamine transporter (PMAT) (*5*). PMAT is different from ENT1−3 in that it does not typically transport nucleosides and nucleoside analogues but rather functions as a polyspecific transporter for a wide range of small hydrophilic organic cations (*5*, *6*). Representative PMAT substrates include the neurotoxin 1-methyl-4-phenylpyridinium (MPP^+) and the monoamine neurotransmitters (e.g., serotonin and dopamine), which are also transported by organic cation transporters (OCTs) in the SLC22 family (*7*−*10*). In humans, PMAT mRNA is most strongly expressed in the brain, and transcripts are also found in other organs such as the kidney, heart, and small intestine (*5*, *11*, *12*). Immunolocalization and biochemical studies suggested that PMAT may play important roles in brain monoamine clearance as well as tissue-specific disposition of organic cations (*13*−*15*).

The human and rodent PMAT proteins consist of ∼530 amino acid residues and were thought to possess an 11-transmembrane domain (TM) topology (*5*, *13*). PMAT (ENT4) is unique in the SLC29 family in that while other SLC29 members (i.e., ENT1−3) are nucleoside transporters, PMAT functions as a polyspecific transporter for structurally diverse organic cations. Despite their distinct substrate specificities, PMAT and ENTs share a similar 11-TM topology, and previous studies have shown that the major substrate recognition sites for PMAT and ENT1 both reside in their N-terminal halves containing TM1−6 (*16*−*18*). Of note, we have previously shown that transplanting TM1−6 of PMAT into ENT1 converted ENT1 from a nucleoside transporter into an organic cation transporter (*16*). On the basis of these data, we hypothesized that PMAT and the ENTs share a similar protein structure, and their distinct substrate specificities are determined by a unique set of residues that line the substrate binding and permeation pathways. Identification of such residues will provide novel insights into the structure−function relationships of transporters in the SLC29 family.

†This work is supported by National Institutes of Health Grant GM066233.

*To whom correspondence should be addressed: Department of Pharmaceutics, Health Sciences Building, Room H272J, University of Washington, 1959 NE Pacific St., Seattle, WA 98195. Telephone: (206) 221-6561. Fax: (206) 543-3204. E-mail: jowang@u.washington.edu.

[1]Abbreviations: PMAT, plasma membrane monoamine transporter; ENT, equilibrative nucleoside transporter; 5-HT, serotonin; MPP^+, 1-methyl-4-phenylpyridinium; OCT, organic cation transporter; WT, wild type; MDCK, Madin−Darby canine kidney; YFP, yellow fluorescence protein; TM, transmembrane domain; NBMPR, nitrobenzylmercaptopurine riboside (nitrobenzylthioinosine).

Published on Web 08/05/2010

Using a series of structurally diverse organic cations, we previously probed the structural requirements of PMAT substrates and inhibitors (*6*). Our analyses revealed that a positive charge and a hydrophobic moiety are the two basic molecular features for transporter−substrate/inhibitor interaction. Interestingly, high-affinity PMAT substrates and inhibitors all possess at least one aromatic ring, whereas cations without a planar aromatic moiety are low-affinity substrates or do not interact with PMAT (*6*). These results suggested that negatively charged residues and aromatic residues may be involved in transporter−substrate recognition through electrostatic interaction and $\pi-\pi$ stacking. Using site-directed mutagenesis, we previously identified a negatively charged residue (E206) on TM5 that functions as a charge sensor and is critical for the cation selectivity of PMAT (*16*).

In this study, we aimed to test the hypothesis that aromatic residues in TM1−6 are involved in substrate recognition and transport. We particularly focused on tyrosine and tryptophan residues because such residues have been implicated in interacting with organic cation substrates (e.g., MPP^+) in the OCTs (*19*, *20*). Tyrosine and tryptophan residues in TM1−6 were first mutated to alanine to identify those essential for PMAT activity. Confocal microscopy and membrane protein biotinylation were used to assess cell surface expression. Additional mutations were introduced at critical positions to further probe the structure−function relationship of PMAT.

EXPERIMENTAL PROCEDURES

Sequence Alignment and Analysis. Sequences of mammalian ENTs were obtained from GenBank with the following accession numbers: hENT1 (AF_079117), rENT1 (NM_031684), mENT1 (AF_218255), macaque ENT1 (AB_168783), canine ENT1 (NM_001003367), cattle ENT1 (NM_001034398), hENT2 (AF_034102), rENT2 (NM_031738), mENT2 (AF_183397), cattle ENT2 (NM_001103269), rabbit ENT2 (AF_323951), hENT3 (AF_326987), rENT3 (AY_273196), mENT3 (AF_326986), cattle ENT3 (NM_001080223), hPMAT (AY_485959), rPMAT (NP_001099381), and mPMAT (NM_146257). ClustalW2 was used for sequence analysis and multiple alignments.

Generation of Mutant Constructs. To facilitate the determination of membrane localization, mutants were constructed using yellow fluorescence protein (YFP)-tagged wild-type (WT) human PMAT as a template. YFP was tagged at the N-termini of the WT and mutant PMAT transporters, and our previous studies have shown that YFP tagging had no effect on the substrate selectivity or kinetic behavior of the transporter (*16*). WT human PMAT was previously subcloned into YFP vector pEYFP-C1 (Clontech, Palo Alto, CA) (*5*). Mutants were generated by site-directed mutagenesis using the QuickChange kit (Stratagene, La Jolla, CA) according to the manufacturer's protocol. The sequence of each mutant was confirmed by direct DNA sequencing in the Department of Biochemistry at the University of Washington.

Stable Expression in MDCK Cells. YFP-tagged mutant constructs were transfected into MDCK cells using Lipofectamine 2000 transfection reagent (Invitrogen, Carlsbad, CA). Stably transfected cell lines were obtained by culturing cells in minimal essential medium containing 10% fetal bovine serum and G418 (1000 μg/mL). Empty vector pEYFP-C1 was transfected into MDCK cells to yield the control cell line. After drug selection for 2−3 weeks, fluorescence-positive cells were purified with a FACS Vantage SE sorter (BD Biosciences, San Jose, CA) at the Cell Analysis Center at the University of Washington. The sorted cells were cultured and maintained in minimal essential medium containing G418 (200 μg/mL).

Confocal Fluorescence Microscopy. To determine the cellular localization of YFP-tagged mutant transporters, $\sim 2 \times 10^5$ cells were grown on top of microscope cover glass in six-well plates (Falcon) for 2−3 days until they were confluent. Cells were mounted onto microscope glass slides with Fluoromount-G (Electron Microscopy Sciences, Hatfield, PA) and visualized with a Leica SP1 confocal microscope equipped with an argon laser as the light source at the Keck Microscopy Facility at the University of Washington. Images were captured by excitation at 488 nm and emission at 515 nm.

Functional Characterization in MDCK Cells. Stably transfected MDCK cells were plated in 24-well plates and allowed to grow for 2−3 days until they were confluent. Growth medium was aspirated, and each well was rinsed once with Krebs-Ringer-Henseleit (KRH) buffer [5.6 mM glucose, 125 mM NaCl, 4.8 mM KCl, 1.2 mM KH_2PO_4, 1.2 mM $CaCl_2$, 1.2 mM $MgSO_4$, and 25 mM HEPES (pH 7.4)] and preincubated in the same buffer for 15 min at 37 °C. Transport assays were performed at 37 °C by incubation of cells in KRH buffer containing a ^{3}H-labeled ligand. [^{3}H]MPP^+ (85 Ci/mmol) and [^{3}H]uridine (30 Ci/mmol) were obtained from American Radiolabeled Chemicals, Inc. (St. Louis, MO). [^{3}H]-5-HT (5-hydroxy[1,2-^{3}H]tryptamine creatinine sulfate, 28.1 Ci/mmol) and [^{3}H]dopamine (3,4-dihydroxy-[2,5,6-^{3}H]phenylethylamine, 51.3 Ci/mmol) were from PerkinElmer Life Sciences, Inc. All other chemicals were obtained from Sigma (St. Louis, MO). For transport studies using ^{3}H-labeled nucleoside uridine, 0.5 μM nitrobenzylmercaptopurine riboside (NBMPR) was added to the transport buffer to suppress endogenous nucleoside uptake activities. For uridine inhibition studies, cells were incubated with ^{3}H-labeled ligands in the presence of 1 mM uridine and transport assays were performed at 37 °C. Uptake was terminated when the cells were washed three times with ice-cold KRH buffer. Cells were then solubilized with 0.5 mL of 1 N NaOH and neutralized with 0.5 mL of 1 N HCl. Radioactivity in the cell lysate was quantified by liquid scintillation counting. The protein concentration in each well was measured using a BCA protein assay kit (Pierce), and the uptake in each well was normalized to its protein content. In all studies, cells transfected with an empty vector served as the background control. Transporter-specific uptake was corrected by subtraction of the background uptake in vector-transfected cells.

Isolation of Plasma Membrane Proteins by Cell Surface Biotinylation. Stably transfected MDCK cells were plated onto 60 mm plates and cultured until they were confluent. Cells were washed twice with 3 mL of ice-cold PBS/CM [138 mM NaCl, 2.7 mM KCl, 8 mM Na_2HPO_4, 1.5 mM KH_2PO_4, 0.1 mM $CaCl_2$, and 1 mM $MgCl_2$ (pH 8.0)]. Biotinylation was conducted on ice by incubation with 1 mL of ice-cold PBS/CM containing a membrane-impermeable biotinylation reagent sulfo-NHS-SS-biotin (0.5 mg/mL) (Pierce, Rockford, IL). After two successive 20 min incubations at 4 °C with freshly prepared NHS-SS-biotin and gentle shaking, cells were briefly rinsed with 3 mL of PBS/CM containing 100 mM glycine. Cells were further incubated at 4 °C with the same solution for 20 min to ensure complete quenching of the unreacted NHS-SS-biotin. Cells were then solubilized on ice via incubation in 1 mL of lysis buffer containing 20 mM Tris, 150 mM NaCl, 1 mM EDTA, 1% Triton X-100, 1 mM phenylmethanesulfonyl fluoride, and Protease Inhibitor Cocktail (Roche) for 1 h with occasional vortexing. Protein

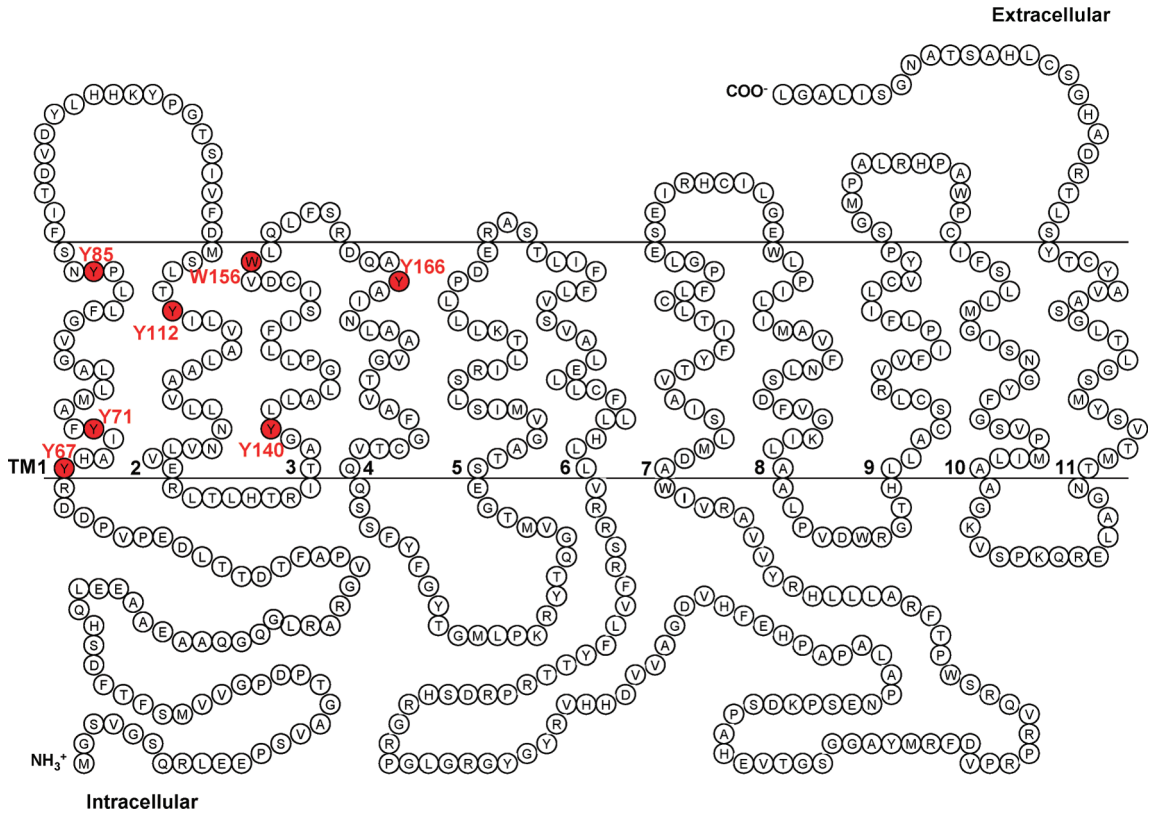

FIGURE 1: Proposed secondary structure of PMAT. Positions of candidate aromatic residues selected for mutagenesis analysis are highlighted in red.

concentrations were measured from the supernatant lysate, and 50 μL of UltraLink Immobilized NeutrAvidin protein (Pierce) was then added to the supernatant for the isolation of membrane proteins. Membrane proteins were subjected to Western blotting using a mouse monoclonal anti-YFP antibody (JL-8) (BD Biosciences) at a 1:1000 dilution, followed by horseradish peroxidase-conjugated goat anti-mouse IgG (1:20000 dilution). The chemiluminescent signals in the Western blots were detected by using SuperSignal West Pico Chemiluminescent Substrate (Pierce) followed by exposure of the blots to X-ray films. Band intensity was quantified by densitometry using ImageQuant (Molecular Dynamics). As reported previously (*16*), double or multiple protein bands around the expected molecular size (~75 kDa) were observed for the YFP-tagged PMAT proteins, which could be due to differential glycosylation of PMAT.

Helical Wheel Analysis. The helical wheels were generated using HelixWheel on the EXPASY molecular biology server and subsequently transposed onto a helical wheel template. The transmembrane domain was assumed to be a standard α-helix (3.6 residues/helical turn). Each residue in TM was plotted every 100° around the center of a circle. The projection of the positions of the residues was shown on a plane perpendicular to the helical axis. Hydrophobicity and hydrophilicity were assigned according to the consensus scale of Eisenberg et al. (*21*).

Data Analysis. For all uptake experiments, data were expressed as means ± the standard deviation (SD) from three independent experiments ($n = 3$) with different cell passages. For each experiment, uptake was conducted in triplicate in three different wells on the same plate. Where applicable, p values were obtained from a Student's t test. For Michaelis−Menten studies, data were fitted to the equation $V = V_{max}[S]/(K_m + [S])$ using Kaleidagraph version 3.6 (Synergy Software, Reading, PA), where V is the transport rate and [S] is the substrate concentration. Kinetic parameters were determined by nonlinear least-squares regression fitting as described previously (*5*, *6*).

RESULTS

Analyses of Tyr and Trp Residues in TM1−6 by Alanine Substitution. PMAT functions as a polyspecific organic cation transporter, and it has been shown that all high-affinity substrates and inhibitors of PMAT possess at least one aromatic ring in their structures (*6*). We thus hypothesized that aromatic residues, especially tyrosine (Tyr) and tryptophan (Trp) in TM1−6, may be involved in substrate recognition and/or translocation. There are six Tyr residues (Y67, Y71, Y85, Y112, Y140, and Y166) and one Trp (W156) on the predicted TM1−4 (Figure 1). No Tyr or Trp was found on TM5 or TM6. All seven residues are completely conserved among human, rat, and mouse PMAT proteins. Alanine (Ala) substitution was first used to test the functional significance of these residues in PMAT function. YFP-tagged mutants Y67A, Y71A, Y85A, Y112A, Y140A, W156A, and Y166A were constructed and stably expressed in MDCK cells. The function of each Ala mutant was analyzed by uptake studies using the prototype PMAT substrates MPP^+, serotonin (5-HT), and dopamine. As shown in Figure 2a, mutation of Y67, Y140, and W156 to Ala largely retained the transport activities for all substrates tested, suggesting that aromatic residues at these three positions are not essential for transporter function. In contrast, mutation of Y71, Y85, Y112, and Y166 to Ala resulted in a substantial loss of transport activities toward all three substrates tested. The loss of the uptake activities of these Ala mutants could be due to impairment of transport function or alteration of cell surface expression levels of the transporter. To differentiate these mechanisms, we

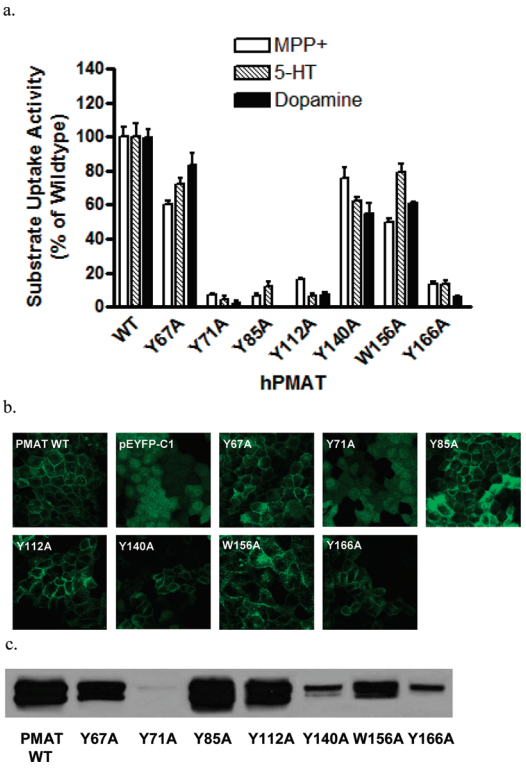

FIGURE 2: (a) Uptake of ^{3}H-labeled MPP$^+$ (1 μM), 5-HT (10 μM), and dopamine (10 μM) by WT PMAT and various alanine mutants in stably transfected MDCK cells. Uptake was performed at 37 °C for 4 min. Substrate uptake was corrected by subtraction of nonspecific uptake in vector-transfected cells. Values are expressed as the percentage of uptake in cells expressing WT PMAT. Each value represents the mean ± SD from three independent experiments (n = 3) with different cell passages. For each experiment, uptake was conducted in triplicate in three different wells on the same plate. (b) Confocal imaging of cellular localization of WT PMAT, pEYFP-C1, and various PMAT alanine mutants in stably transfected MDCK cells. (c) Plasma membrane expression of WT PMAT and various PMAT alanine mutants detected by biotinylation followed by Western blotting with an anti-YFP monoclonal antibody.

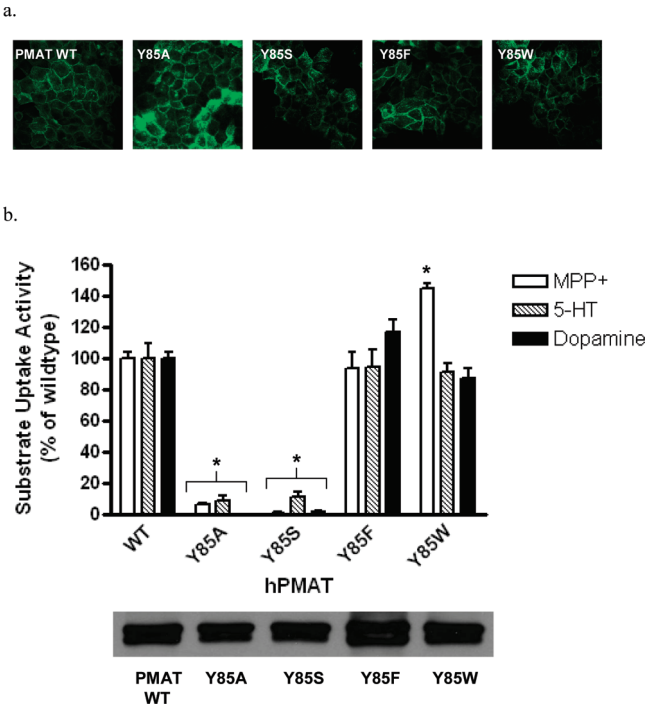

FIGURE 3: (a) Confocal imaging of cellular localization of WT PMAT and various Y85 mutants in stably transfected MDCK cells. (b) Uptake of ^{3}H-labeled MPP$^+$ (1 μM), 5-HT (10 μM), and dopamine (10 μM) by WT PMAT and various Y85 mutants in stably transfected MDCK cells (top, histogram). Uptake was performed at 37 °C for 4 min. Substrate uptake was corrected by subtraction of nonspecific uptake in vector-transfected cells. Values are expressed as the percentage of uptake in cells expressing WT PMAT. Each value represents the mean ± SD from three independent experiments (n = 3) with different cell passages. For each experiment, uptake was conducted in triplicate in three different wells on the same plate. Asterisks denote $p < 0.01$, vs WT values. Plasma membrane expression of WT PMAT and various Y85 mutants detected by biotinylation followed by Western blot with an anti-YFP monoclonal antibody (bottom, gel).

visualized cellular localizations of the Ala mutants by confocal microscopy and detected their plasma membrane expression levels by cell surface biotinylation followed by Western blot analysis. As shown in panels b and c of Figure 2, the three functional mutants (Y67A, Y140A, and W156A) were localized on the plasma membrane. In contrast, mutant Y71A, which lost organic cation transport activity, exhibited diffused fluorescence throughout the cytoplasm (Figure 2b), with no detectable protein on the plasma membrane (Figure 2c). Mutant Y166A showed some plasma membrane localization, but the cell surface expression level was only approximately one-tenth of that of WT PMAT. These data suggest that the loss of organic cation transport activity in cells expressing Y71A and Y166A was mainly due to problems in PMAT protein stability and/or membrane trafficking. Importantly, two mutants, Y85A and Y112A, exhibited normal plasma membrane expressions but lost uptake activities toward organic cations (Figure 2), suggesting that substitution of Tyr with Ala at these two positions affected the catalytic activity of the transporter. Y85 and Y112 were predicted to be located within TM1 and TM2, respectively. These two potentially important aromatic residues were chosen for more detailed analyses.

Effect of Side Chain Substitution at Y85. To investigate whether an aromatic side chain is essential for PMAT function at position 85, we mutated Tyr to Trp and Phe. Tyrosine was also changed to serine (Ser), a residue that retains a hydroxyl group but lacks an aromatic feature. Y85S, Y85F, and Y85W were constructed and stably expressed in MDCK cells. All mutants exhibited plasma membrane expression patterns similar to that of WT PMAT (Figure 3a). Cell surface biotinylation followed by Western blot analysis revealed that the membrane expression levels of all Y85 mutant proteins were comparable to that of WT PMAT (Figure 3b, bottom panel). Functional assays showed that substitution of Y85 with nonaromatic residues (Y85A and Y85S) resulted in the nearly complete loss of activities toward all substrates tested (Figure 3b, top panel). In contrast, substitution of Y85 with aromatic residues (Y85F and Y85W) fully restored transporter activities (Figure 3b, top panel). Interestingly, compared to WT PMAT, mutant Y85W exhibited similar activities toward 5-HT and dopamine, but a significantly higher transport rate toward MPP$^+$ (Figure 3b, top panel).

Effect of Side Chain Substitution at Y112. Y112S, Y112F, and Y112W were constructed and stably expressed in MDCK cells. All mutants exhibited plasma membrane localization (Figure 4a). The levels of cell surface expression of Y112A, Y112S, and Y112F were comparable to that of WT PMAT, while Y112W showed a slightly higher (~1.7-fold) level of expression (Figure 4b, bottom panel). Functional assays showed that substitution of Y112 with nonaromatic residues (Y112A and

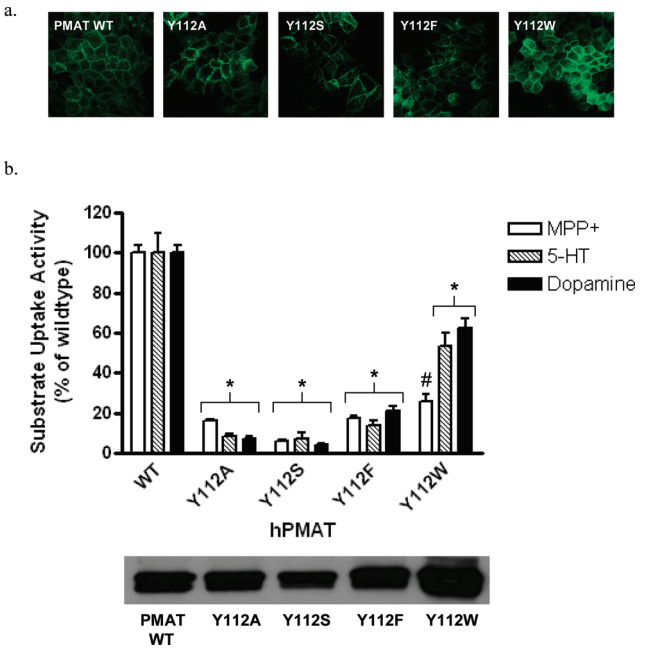

FIGURE 4: (a) Confocal imaging of cellular localization of WT PMAT and various Y112 mutants in stably transfected MDCK cells. (b) Uptake of ^{3}H-labeled MPP$^+$ (1 μM), 5-HT (10 μM), and dopamine (10 μM) by WT PMAT and various Y112 mutants in stably transfected MDCK cells (top, histogram). Uptake was performed at 37 °C for 4 min. Substrate uptake was corrected by subtraction of nonspecific uptake in vector-transfected cells. Values are expressed as the percentage of uptake in cells expressing WT PMAT. Each value represents the mean ± SD from three independent experiments (n = 3) with different cell passages. For each experiment, uptake was conducted in triplicate in three different wells on the same plate. Asterisks denote $p < 0.01$, vs WT values. Number signs denote $p < 0.01$, vs Y112W-mediated 5-HT and dopamine uptake values. Plasma membrane expression of WT PMAT and various Y112 mutants detected by biotinylation followed by Western blot with an anti-YFP monoclonal antibody (bottom, gel).

Y112S) resulted in an ~90% loss of transporter activities toward all organic cations tested (Figure 4b, top panel). Mutant Y112F showed only < 20% activities toward all tested substrates, suggesting that substitution of Tyr with Phe is not allowed at position 112. Interestingly, Trp substitution at Y112 appeared to have a differential impact on transport activities toward MPP$^+$, 5-HT, and dopamine (Figure 4b, top panel). Compared to cells expressing WT PMAT, cells expressing Y112W retained 50−60% activities toward 5-HT and dopamine. However, much less (~20%) activity was retained for MPP$^+$. These data suggest that Y112 in TM2 plays a specific role in interacting with organic cation substrates, and the effect of Trp substitution at this position is substrate-dependent.

Transport Kinetics of Mutants Y85W and Y112W. While Trp substitution was allowed at position Y85 and partially permitted at position Y112, the impacts of these side chain changes on transport activities appeared to be substrate-dependent (Figures 3b and 4b). To understand the kinetic mechanisms underlying such observations, we performed detailed kinetic analyses on WT PMAT and mutants Y85W and Y112W (Figure 5). The resulting kinetic parameters (summarized in Table 1) clearly demonstrated that Tyr to Trp substitution at both positions differentially influenced the transport kinetics of MPP$^+$, 5-HT, and dopamine. For MPP$^+$, the Y85W substitution produced a 1.6-fold increase in maximal velocity (V_{max}), with little effect on apparent binding affinity (K_m), resulting in

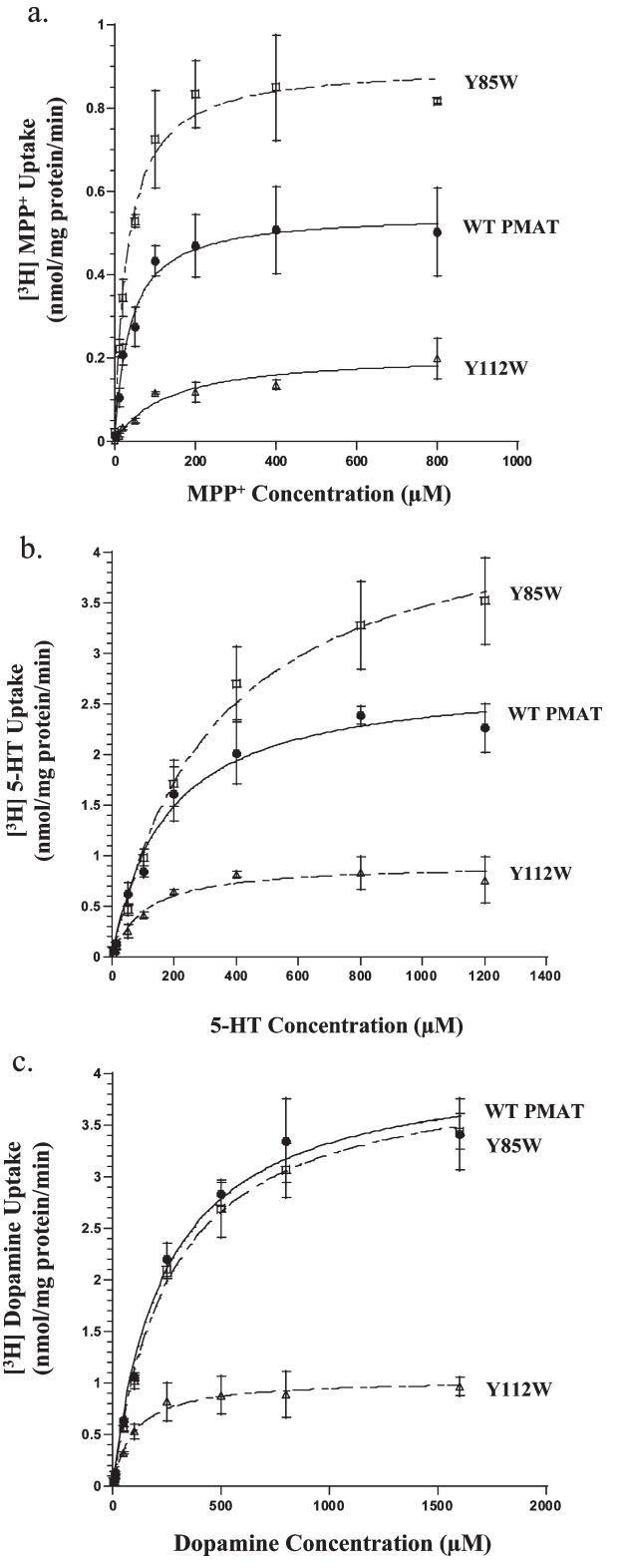

FIGURE 5: Concentration-dependent transport of (a) MPP$^+$, (b) 5-HT, and (c) dopamine by WT PMAT, Y85W, and Y112W. Vector-, WT PMAT-, Y85W-, and Y112W-transfected MDCK cells were incubated with varying concentrations of the substrates for 1 min at 37 °C. Specific uptake was calculated by subtraction of the uptake values in vector-transfected cells. WT PMAT (●), Y85W (□), and Y112W (△) concentration-dependent uptake values are shown. Each value represents the mean ± SD from three independent experiments (n = 3) with different cell passages. For each experiment, uptake was conducted in triplicate in three different wells on the same plate.

an ~2-fold increase in transport efficiency (V_{max}/K_m) toward MPP$^+$ (Figure 5a and Table 1). For 5-HT, Y85W substitution

Table 1: Transport Kinetics of WT PMAT and Mutants Y85W and Y112W[a]

	MPP$^+$			serotonin			dopamine		
	K_m (μM)	V_{max} [nmol (mg of protein)$^{-1}$ min^{-1}]	V_{max}/K_m	K_m (μM)	V_{max} [nmol (mg of protein)$^{-1}$ min^{-1}]	V_{max}/K_m	K_m (μM)	V_{max}[nmol (mg of protein)$^{-1}$ min^{-1}]	V_{max}/K_m
wild type	42.2 ± 5.0	0.60 ± 0.04	0.014 ± 0.002	167.5 ± 18.9	2.80 ± 0.24	0.017 ± 0.002	244.4 ± 16.2	4.12 ± 0.35	0.017 ± 0.002
Y85W	31.1 ± 6.9	0.94 ± 0.10[b]	0.030 ± 0.007[c]	308.2 ± 50.8[c]	4.08 ± 0.30[b]	0.013 ± 0.002	242.6 ± 30.4	3.87 ± 0.14	0.016 ± 0.002
Y112W	146.8 ± 36.3[b]	0.23 ± 0.02[b]	0.002 ± 0.0004[b]	103.9 ± 13.2[b]	1.04 ± 0.13[b]	0.010 ± 0.002[c]	88.0 ± 6.8[b]	1.03 ± 0.09[b]	0.012 ± 0.001[c]

[a]All experiments were performed in triplicate in three different wells on the same plate and repeated three times. Values are expressed as means ± SD from parameters obtained from three independent experiments (n = 3) with different cell passages. [b]$p < 0.01$ vs WT PMAT values. [c]$p < 0.05$ vs WT PMAT values.

caused a similar degree of increase in both K_m and V_{max}, leading to an unaltered transport efficiency toward this substrate (Figure 5b and Table 1). For dopamine, the Y85W substitution had no effect on either K_m or V_{max} (Figure 5c and Table 1). At position Y112, Trp substitution produced a marked (2.6−4-fold) reduction in V_{max} for all three tested substrates, suggesting a universal impairment in the transporter's turnover rate (Table 1). Remarkably, the effect on K_m was largely substrate-dependent. For MPP$^+$, a 2.6-fold reduction in V_{max} was accompanied by a significant increase (3.5-fold) in K_m, resulting in a substantial (7-fold) reduction in MPP$^+$ transport efficiency (V_{max}/K_m) (Figure 5a and Table 1). However, for 5-HT and dopamine, the reduction in V_{max} was compensated by a simultaneous decrease in K_m, resulting in transport efficiencies that were still 60−70% of that of WT PMAT (Figure 5b,c and Table 1). These data are consistent with the results from single-concentration uptake studies performed at a low substrate concentration (Figure 4b) and further demonstrate the importance of Y112 in recognizing and transporting MPP$^+$. Together, these results confirmed that Trp substitution at Y85 and Y112 influenced substrate binding and/or transport in a substrate-dependent manner, and these two residues may play specific roles in interacting with the substrates.

Uridine Uptake and Interaction with PMAT Mutants. Sequence alignments showed that at the equivalent positions of Y85, a Trp residue is conserved in all ENT1−3 forms from various species (Figure 6a). At the equivalent position of Y112 in PMAT, the Tyr residue is substituted with an Ala residue in ENT1 transporters and a Ser residue in ENT2 and ENT3 isoforms (Figure 6a). We thus tested whether mutating Y85 and Y112 to their corresponding residues in ENT1 or ENT2 would lead to a gain of transport activity toward uridine, a prototypical substrate for the ENTs. Like WT PMAT, Y85W, Y112A, and Y112S mutants exhibited no statistically significant transport activities for uridine (Figure 6b). In addition, no significant inhibitory effect of uridine (1 mM) was observed for Y85W-mediated organic cation transport (data not shown). These data suggest that single substitution with an ENT1 or -2 equivalent residue at these positions is not sufficient to enhance interaction of PMAT with nucleosides.

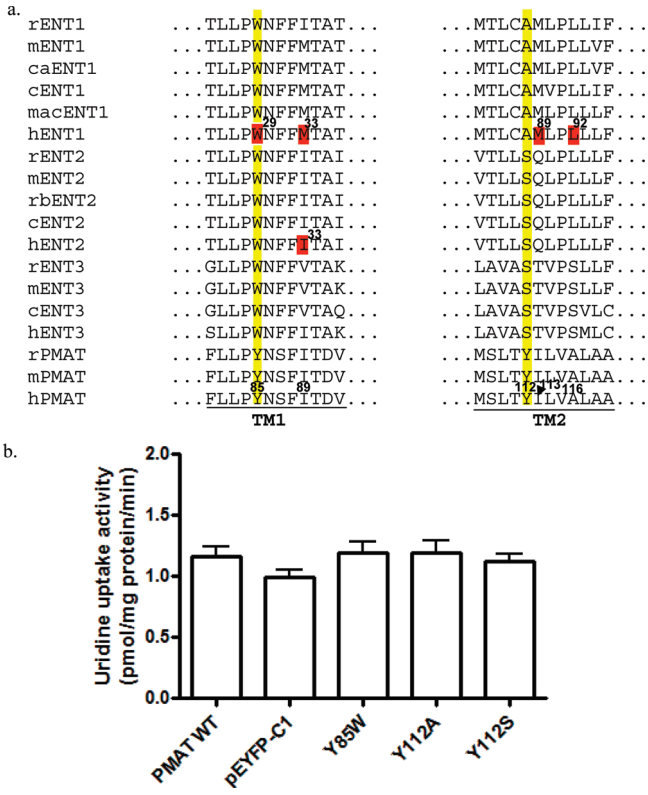

FIGURE 6: (a) Multiple-sequence alignments of PMATs with mammalian ENTs in TM1 and TM2 regions. Y85 and Y112 in PMATs and their corresponding residues in ENTs are numbered and highlighted in yellow. Functionally important residues previously identified in ENTs are numbered and highlighted in red. Corresponding residues in human PMAT are numbered (r, rat; m, mouse; ca, canine; c, cattle; mac, macaques; h, human; rb, rabbit). (b) Uptake of uridine in the presence of NBMPR by various PMAT mutants in stably transfected MDCK cells. Values are expressed as picomoles per milligram of protein per minute. Each value represents the mean ± SD from three independent experiments (n = 3) with different cell passages. For each experiment, uptake was conducted in triplicate in three different wells on the same plate. There was no statistically significant difference in uridine transport for WT and mutant PMAT proteins as compared to the pEYFP-C1 vector-transfected cells.

DISCUSSION

Previous structure−activity studies on PMAT suggested the possible involvement of aromatic residues in high-affinity interaction with substrates (*6*). In this study, we aimed to identify these residues. We confined our analyses with TM1−6 as our previous studies suggested that the major substrate recognition sites of PMAT are contained within this region (*16*). Among the three aromatic residues (Tyr, Trp, and Phe), Tyr and Trp were previously shown to be involved in interaction with organic cation substrates (e.g., MPP$^+$) by the OCTs (*19*, *20*), which share a large substrate overlap with PMAT (*6*). Additionally, as PMAT substrates are mostly hydrophilic cations, we suspect that Phe may be too hydrophobic to directly interact with organic cations in an aqueous pore. Therefore, we specifically focused on Tyr and Trp in this study.

We first analyzed the six Tyr residues and one Trp residue on TM1−6 by alanine substitution (Figure 2). Our results showed

that Ala replacement at Y67, Y140, and W156 did not significantly affect transporter activities, suggesting that these residues are not essential for PMAT function. It is also noted that mutant Y140A exhibited a relatively normal transport activity toward various organic cations despite a significantly lower level of cell surface expression. This could imply an enhanced affinity for substrates and/or a higher intrinsic transport activity compared to that of WT PMAT, leading to the apparently "normal" transport rate toward the tested substrates. Alanine substitution at Y71 and Y166 impaired PMAT cell surface expression, suggesting Tyr residues at these two positions are important for protein stability and/or membrane targeting. Importantly, alanine substitution at Y85 and Y112 resulted in normal plasma membrane expressions but nearly complete loss of transport activities, suggesting that Y85 and Y112 are crucial for the transport function of PMAT.

To further probe the structural requirement at Y85 and Y112, additional mutational analyses were conducted. Our results showed that at Y85, aromatic substitution with Trp or Phe could fully restore PMAT activity whereas nonaromatic replacement (e.g., Ala or Ser) was not allowed (Figure 3). These data suggest that the presence of an aromatic side chain at position Y85 is essential for PMAT function. Detailed analyses further revealed that the effect of Trp substitution at Y85 influenced transport kinetics in a substrate-dependent manner (Figure 5 and Table 1). Interestingly, multiple-sequence alignments showed that at the position equivalent to Y85, a Trp residue is conserved among all other members of the SLC29 family, ENT1−3 (Figure 6a). It should be noted that nucleosides also contain at least one heterocyclic aromatic ring on the purine or pyrimidine base. In human ENT1, random mutagenesis studies have identified Trp29 as an important determinant of hENT1 nucleoside selectivity and may interact with nucleosides and nucleoside inhibitor via ring stacking interactions (*22*). Trp29 lies close to Met33, another functionally important component of the substrate/inhibitor binding site in ENT1 (*23*). Met33 is responsible for the high-affinity binding of hENT1 to its classic inhibitor NBMPR, whereas isoleucine substitution (Ile33) in hENT2 underlies its low sensitivity to the inhibitor (*23*, *24*). Helical wheel analysis revealed that in PMAT, Y85 (corresponding to W29 in hENT1) is close to I89 (corresponding to M33 in hENT1 and I33 in hENT2), occupying a position that is known to form part of the substrate/inhibitor binding site in the ENTs (Figure 7a). These data suggest that Y85 and TM1 in PMAT are important components of the substrate recognition and permeation pathway. Y85 may recognize an aromatic feature in PMAT substrates presumably through $\pi-\pi$ interaction. Alternatively, the residue may be structurally involved in forming the substrate recognition and translocation pathway, possibly through interacting with other nearby aromatic residues via ring stacking interactions.

Y112 on TM2 is indispensable for the organic cation transport function of PMAT. Nonaromatic replacements (Y112A and Y112S) were not allowed (Figure 4). Even conservative substitution with Phe, which differs from Tyr only in missing a hydroxyl group on the phenyl ring, resulted in a nonfunctional transporter (Figure 4). These data suggest that at position 112, both a hydroxyl group and an aromatic ring are necessary for normal transporter function. The specific role of the phenolic hydroxyl group is less clear, but it may act as an electron donor to stabilize the positive charge carried by an organic cation substrate. Interestingly, Trp substitution at Y112 partially restored transport activities toward 5-HT and dopamine but severely impaired

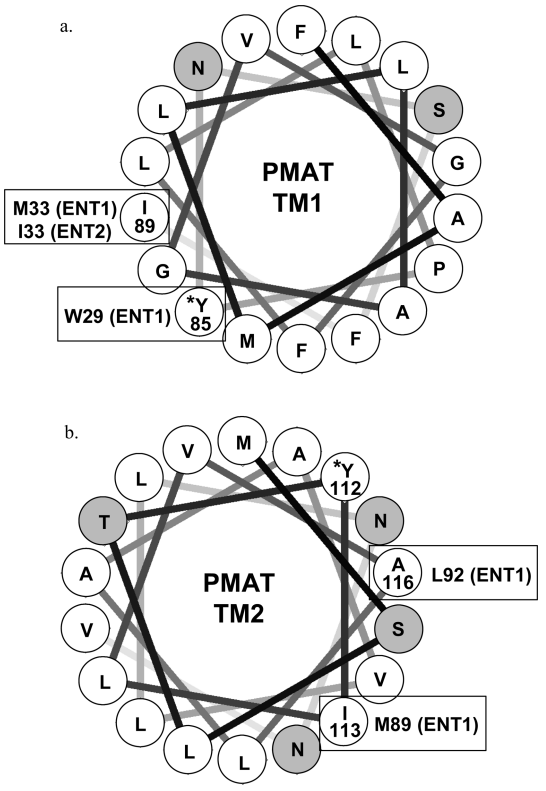

FIGURE 7: Helical wheel analysis of (a) TM1 and (b) TM2 of PMAT. The transmembrane domains are assumed to be standard α-helix, and each residue is plotted every 100° around the center of a circle. The figures show the projection of the positions of the residues on a plane perpendicular to the helical axis. Hydrophobic residues are colored white, and hydrophilic residues are colored gray. Residues in PMAT identified as being functionally important in this study are marked with asterisks. Functionally important residues previously identified in ENT1 and/or ENT2 with positions corresponding or close to Y85 and Y112 in PMAT are boxed.

MPP^+ transport (Figure 4). Detailed kinetic analyses revealed that mutant Y112W showed a universal reduction in its V_{max} toward all three tested substrates, suggesting that the Tyr residue at this position is essential for the optimal organic cation transport function of PMAT. Our kinetic studies also uncovered the fact that the substantial reduction in MPP^+ transport activity observed in mutant Y112W was due to dual impairments in apparent binding affinity (i.e., increase in K_m) and maximal transport velocity (V_{max}) (Table 1). On the other hand, for 5-HT and dopamine, reductions in V_{max} were partially compensated by simultaneous increases in binding affinity (i.e., decrease in K_m), which resulted in transport efficiencies that were ~60−70% of that of WT PMAT. This substrate-dependent effect implies that multiple substrate binding sites may exist within the translocation pathway. Given that the substrate specificity of PMAT is broad and includes a variety of compounds with diverse structures, it is likely that PMAT protein may contain a promiscuous binding pocket in which conservative substitution of key residues may have a different impact on the binding and transport of different substrates. Multiple-sequence alignments showed that at the position equivalent to Y112, ENT1 transporters possess an Ala while ENT2 and ENT3 contain a Ser residue (Figure 6a). The roles of these residues in ENT function have not been analyzed. However, M89 and L92 in hENT1 TM2 have been shown to be important for nucleoside and inhibitor interactions (*25*, *26*). M89 and L92 in hENT1 correspond to I113 and A116 in PMAT,

respectively (Figure 6a). Helical wheel analysis suggests that Y112, I113, and A116 in PMAT are located in the proximity of one another on the same hemisphere of TM2 (Figure 7b). These data suggest that TM2 in PMAT participates in formation of the organic cation permeation pathway and Y112 specifically interacts with organic cations through both its aromatic ring and phenolic hydroxyl group.

In summary, we have identified Y85 and Y112 as being crucial for the catalytic activities and substrate selectivities of PMAT. Y112 may specifically interact with organic cation substrates via its phenolic hydroxyl group. Together with previous findings (*16*), the data suggest that TM1, TM2, and TM5 are critical constituents of the substrate permeation pathway in PMAT. Although the proposed secondary structure of PMAT (Figure 1) awaits experimental validation, results from our recent immunocytochemistry studies, using two epitope-specific polyclonal antibodies directed toward the predicted N-terminus and the last intracellular loop, were in good agreement with the proposed 11-TM model (*12*, *14*). The 11-TM model has been experimentally confirmed in ENT1 (*27*), and TM1, TM2, and TM5 were also previously shown to be important components of the substrate recognition and translocation pathway in ENT1 (*22*, *23*, *25*, *26*). Thus, our results indicate that PMAT and the ENT proteins share a similar tertiary structure, and the unique substrate selectivity of PMAT is due to evolutionary replacement of a set of key residues in the substrate recognition domains of the transporter.

REFERENCES

1. Kong, W., Engel, K., and Wang, J. (2004) Mammalian nucleoside transporters. *Curr. Drug Metab. 5*, 63–84.
2. Baldwin, S. A., Beal, P. R., Yao, S. Y., King, A. E., Cass, C. E., and Young, J. D. (2004) The equilibrative nucleoside transporter family, SLC29. *Pfluegers Arch. 447*, 735–743.
3. Baldwin, S. A., Yao, S. Y., Hyde, R. J., Ng, A. M., Foppolo, S., Barnes, K., Ritzel, M. W., Cass, C. E., and Young, J. D. (2005) Functional characterization of novel human and mouse equilibrative nucleoside transporters (hENT3 and mENT3) located in intracellular membranes. *J. Biol. Chem. 280*, 15880–15887.
4. Govindarajan, R., Leung, G. P., Zhou, M., Tse, C. M., Wang, J., and Unadkat, J. D. (2009) Facilitated mitochondrial import of antiviral and anticancer nucleoside drugs by human equilibrative nucleoside transporter-3. *Am. J. Physiol. 296*, G910–G922.
5. Engel, K., Zhou, M., and Wang, J. (2004) Identification and characterization of a novel monoamine transporter in the human brain. *J. Biol. Chem. 279*, 50042–50049.
6. Engel, K., and Wang, J. (2005) Interaction of organic cations with a newly identified plasma membrane monoamine transporter. *Mol. Pharmacol. 68*, 1397–1407.
7. Fujita, T., Urban, T. J., Leabman, M. K., Fujita, K., and Giacomini, K. M. (2006) Transport of drugs in the kidney by the human organic cation transporter, OCT2 and its genetic variants. *J. Pharm. Sci. 95*, 25–36.
8. Koepsell, H., and Endou, H. (2004) The SLC22 drug transporter family. *Pfluegers Arch. 447*, 666–676.
9. Wright, S. H., and Dantzler, W. H. (2004) Molecular and cellular physiology of renal organic cation and anion transport. *Physiol. Rev. 84*, 987–1049.
10. Zhang, L., Brett, C. M., and Giacomini, K. M. (1998) Role of organic cation transporters in drug absorption and elimination. *Annu. Rev. Pharmacol. Toxicol. 38*, 431–460.
11. Zhou, M., Xia, L., and Wang, J. (2007) Metformin transport by a newly cloned proton-stimulated organic cation transporter (plasma membrane monoamine transporter) expressed in human intestine. *Drug Metab. Dispos. 35*, 1956–1962.
12. Xia, L., Zhou, M., Kalhorn, T. F., Ho, H. T., and Wang, J. (2009) Podocyte-specific expression of organic cation transporter PMAT: Implication in puromycin aminonucleoside nephrotoxicity. *Am. J. Physiol. 296*, F1307–F1313.
13. Dahlin, A., Xia, L., Kong, W., Hevner, R., and Wang, J. (2007) Expression and immunolocalization of the plasma membrane monoamine transporter in the brain. *Neuroscience 146*, 1193–1211.
14. Xia, L., Engel, K., Zhou, M., and Wang, J. (2007) Membrane localization and pH-dependent transport of a newly cloned organic cation transporter (PMAT) in kidney cells. *Am. J. Physiol. 292*, F682–F690.
15. Zhou, M., Engel, K., and Wang, J. (2007) Evidence for significant contribution of a newly identified monoamine transporter (PMAT) to serotonin uptake in the human brain. *Biochem. Pharmacol. 73*, 147–154.
16. Zhou, M., Xia, L., Engel, K., and Wang, J. (2007) Molecular determinants of substrate selectivity of a novel organic cation transporter (PMAT) in the SLC29 family. *J. Biol. Chem. 282*, 3188–3195.
17. Sundaram, M., Yao, S. Y., Ng, A. M., Griffiths, M., Cass, C. E., Baldwin, S. A., and Young, J. D. (1998) Chimeric constructs between human and rat equilibrative nucleoside transporters (hENT1 and rENT1) reveal hENT1 structural domains interacting with coronary vasoactive drugs. *J. Biol. Chem. 273*, 21519–21525.
18. Yao, S. Y., Ng, A. M., Vickers, M. F., Sundaram, M., Cass, C. E., Baldwin, S. A., and Young, J. D. (2002) Functional and molecular characterization of nucleobase transport by recombinant human and rat equilibrative nucleoside transporters 1 and 2. Chimeric constructs reveal a role for the ENT2 helix 5−6 region in nucleobase translocation. *J. Biol. Chem. 277*, 24938–24948.
19. Popp, C., Gorboulev, V., Muller, T. D., Gorbunov, D., Shatskaya, N., and Koepsell, H. (2005) Amino acids critical for substrate affinity of rat organic cation transporter 1 line the substrate binding region in a model derived from the tertiary structure of lactose permease. *Mol. Pharmacol. 67*, 1600–1611.
20. Gorboulev, V., Shatskaya, N., Volk, C., and Koepsell, H. (2005) Subtype-specific affinity for corticosterone of rat organic cation transporters rOCT1 and rOCT2 depends on three amino acids within the substrate binding region. *Mol. Pharmacol. 67*, 1612–1619.
21. Eisenberg, D., Wilcox, W., and McLachlan, A. D. (1986) Hydrophobicity and amphiphilicity in protein structure. *J. Cell. Biochem. 31*, 11–17.
22. Paproski, R. J., Visser, F., Zhang, J., Tackaberry, T., Damaraju, V., Baldwin, S. A., Young, J. D., and Cass, C. E. (2008) Mutation of Trp29 of human equilibrative nucleoside transporter 1 alters affinity for coronary vasodilator drugs and nucleoside selectivity. *Biochem. J. 414*, 291–300.
23. Visser, F., Vickers, M. F., Ng, A. M., Baldwin, S. A., Young, J. D., and Cass, C. E. (2002) Mutation of residue 33 of human equilibrative nucleoside transporters 1 and 2 alters sensitivity to inhibition of transport by dilazep and dipyridamole. *J. Biol. Chem. 277*, 395–401.
24. Visser, F., Zhang, J., Raborn, R. T., Baldwin, S. A., Young, J. D., and Cass, C. E. (2005) Residue 33 of human equilibrative nucleoside transporter 2 is a functionally important component of both the dipyridamole and nucleoside binding sites. *Mol. Pharmacol. 67*, 1291–1298.
25. Endres, C. J., and Unadkat, J. D. (2005) Residues Met89 and Ser160 in the human equilibrative nucleoside transporter 1 affect its affinity for adenosine, guanosine, S6-(4-nitrobenzyl)-mercaptopurine riboside, and dipyridamole. *Mol. Pharmacol. 67*, 837–844.
26. Endres, C. J., Sengupta, D. J., and Unadkat, J. D. (2004) Mutation of leucine-92 selectively reduces the apparent affinity of inosine, guanosine, NBMPR [S6-(4-nitrobenzyl)-mercaptopurine riboside] and dilazep for the human equilibrative nucleoside transporter, hENT1. *Biochem. J. 380*, 131–137.
27. Sundaram, M., Yao, S. Y., Ingram, J. C., Berry, Z. A., Abidi, F., Cass, C. E., Baldwin, S. A., and Young, J. D. (2001) Topology of a human equilibrative, nitrobenzylthioinosine (NBMPR)-sensitive nucleoside transporter (hENT1) implicated in the cellular uptake of adenosine and anti-cancer drugs. *J. Biol. Chem. 276*, 45270–45275.